Corrosion Science 249 (2025) 112824

Contents lists available at ScienceDirect

Corrosion Science

journal homepage: www.elsevier.com/locate/corsci

# Experimental approach and assessment of Zr conversion coatings on Al alloy using response surface methodology

Ana Kraš [a,b], Davorin Kramar [c], Ingrid Milošev [a,b,*,1]

[a] Jožef Stefan Institute, Department of Physical and Organic Chemistry, Jamova c. 39, Ljubljana SI–1000, Slovenia
[b] Jožef Stefan International Postgraduate School, Jamova c. 39, Ljubljana SI–1000, Slovenia
[c] University of Ljubljana, Faculty of Mechanical Engineering, Laboratory for Quality Assurance, Aškerčeva 6, Ljubljana SI–1000, Slovenia

ARTICLE INFO

*Keywords:*
A. aluminium
B. EIS
C. response surface methodology
D. conversion coatings

ABSTRACT

This study extended the use of response surface methodology (RSM) to explore the experimental space, identify optimal conditions for deposition and drying, and assess factor interactions for zirconium conversion coatings on aluminium alloy 5754. Corrosion resistance in a dilute Harrison's solution was evaluated using a non-electrochemical drop test and electrochemical techniques. Surface analysis supported the electrochemical findings obtained with the chosen RSM conditions. Unlike zinc and cold-rolled steel, AA5754 exhibits heightened sensitivity to the interplay of pH, conversion time, and $H_2ZrF_6$ concentration, which is attributed to the presence of intermetallic particles governing cathodic reactions and the subsequent conversion processes.

## 1. Introduction

It seems that practically important knowledge about zirconium conversion coatings (ZrCCs) is primarily documented in industrial reports and patents. Despite being accessible through databases, these sources are often restricted by paywalls, written in complex language, and frequently lack essential information needed for a fundamental understanding of their mechanisms. This, in turn, hinders the identification of pathways for improvement. Adding to the challenge, most scientific articles concerning ZrCCs primarily focus on evaluating and reporting their performance compared to prior literature findings. In this context, they often employ commercial ZrCCs with undisclosed compositions while paying little to no attention to the chemistry of Zr or other ZrCC bath additives. Building upon the insights from our comprehensive investigation into zirconium conversion coatings on cold-rolled steel (CRS) and zinc [1], this article extends the exploration to the traditional focus on aluminium alloys. Specifically, AA5754 was chosen due to its use as a substrate in the automotive industry [2]. This article continues our previous studies on thermodynamic and electrochemical studies on zirconium conversion coatings on CRS, Zn and AA5754 [3,4].

The Design of Experiment (DoE) methodologies [5], particularly response surface methodology (RSM) [6,7], which has proven effective in our previous study, continue to guide our exploration of AA5754. This contrasts with the One Factor at a Time (OFAT) approach, which isolates one factor, risking a limited exploration of the experimental space and overlooking potential factor interactions [5,7]. While Zn and CRS demonstrate comparable corrosion behaviour in ZrCCs [1,8], resulting in visually uniform deposition [1], aluminium alloys introduce an added complexity by containing various intermetallic particles (IMPs). The latter often act as cathodic sites of increased alkalinity due to oxygen reduction reaction and consequent initiation sites for the precipitation conversion of zirconium species from the solution to the metal surface. This contributes to the development of notably thicker ZrCCs on these particles, yielding an inhomogeneous coating that is further susceptible to electrolyte leaching. Most studies on ZrCC were conducted on AAs of series 2xxx and 6xxx, while comparative studies on series 5xxx are relatively scarce [8,9]. Our previous study showed that ZrCC deposited in the conversion bath of 200 ppm $H_2ZrF_6$ for 10 min provided good corrosion protection for AA5754 in 0.5 M NaCl with impedance values at the frequency of 3 mHz in the range of MΩ $cm^2$ after 3 days of immersion in 0.5 M NaCl [9]. AA5754 contains mainly $(MnFe)Al_6$ with a much higher ratio of Fe/Mn = 7.8, with a Fe/Mn ratio of 0.8. Both IMPs are noble relative to the alloy's matrix and act as local cathodes [9]. Consequently, it is expected that AA5754, will be even more sensitive to changes in conversion bath parameters than CRS and Zn [1] due to

* Correspondence to: Department of Physical and Organic Chemistry, Jožef Stefan Institute, Jamova 39, Ljubljana SI-1000, Slovenia.
*E-mail address:* ingrid.milosev@ijs.si (I. Milošev).
[1] URL: https://www.ijs.si/ijsw/K3-en/Milosev

https://doi.org/10.1016/j.corsci.2025.112824
Received 24 November 2024; Received in revised form 11 February 2025; Accepted 24 February 2025
Available online 25 February 2025

different deposition mechanisms, with coatings being much thicker above IMPs (in the micron range) compared to the alloy matrix (in the nanometer range) [8–11].

In brief, RSM enables modelling relationships between multiple factors and the chosen response. It identifies factor interactions and determines whether the relationship is linear, quadratic, or more complex [6,7]. The three most influential factors in the ZrCC process defined after literature screening—pH, concentration, and conversion time [9–12]—should be investigated for their independent and interactive contributions. However, the primary challenge lies in adequately testing such thin coatings (thickness typically ranging between 10 and 50–80 nm [8]).

To address this, a comparison should be made between destructive electrochemical techniques, such as potentiodynamic polarisation curves (PPC), and non-destructive electrochemical techniques, like electrochemical impedance spectroscopy (EIS) [13,14], along with an independent, non-electrochemical technique, such as "drop test" [15]. This comprehensive approach is crucial for a thorough understanding and assessment of ZrCC's behaviour and performance. Further issues worth considering are the type of solution used to obtain relevant responses. Typically, air drying stands out as the most straightforward post-treatment method for water-based coatings. Choosing the most appropriate corrosion protection assessment technique and selecting an electrolyte for electrochemically-based studies also add complexity to the process. Considering these factors is essential for a thorough and precise analysis, a consideration central to this study. Using a dilute Harrison's solution (DHS) [16] has been suggested as appropriate for providing the trade-off between the aggressiveness of typical corrosion test electrolytes and the corrosion resistance of most substrates.

The aim of using RSM is to enhance the corrosion protection of ZrCCs and overcome challenges in evaluating thin film corrosion using electrochemical techniques and other assessment methods. RSM results in our previous study [1] indicate that conducting a drop test and EIS immediately post-conversion for CRS and after 24-hour air-drying for Zn can be an effective non-destructive screening method for ZrCC behaviour. Furthermore, polarisation resistance from PPC was found to be a more convenient response than corrosion current density. EIS indicated that charge transfer resistance controls ZrCC corrosion on CRS, while diffusion control prevails on Zn. Additionally, a high-frequency time constant in EIS spectra on CRS suggested better corrosion protection and satisfactory ZrCC formation. On the other hand, on Zn at pH $\geq 4$, EIS describes ZrCC thickness through the diffusion time constant, while at pH $< 4$, EIS captures the behaviour of porous ZnO formed during conversion.

With the increased sensitivity of aluminium alloys to process parameters, it is reasonable to anticipate that the full utilisation of RSM, leading to the confirmation of predicted optimal results as observed in our previous study, may not be achievable. However, this does not preclude using RSM to evaluate and compare techniques in a manner similar to our previous study.

Using this interconnected approach, we believe that a cohesive understanding of ZrCC performance on various substrates can be achieved, paving the way for the development of robust and versatile alternatives to traditional chromate conversion coatings (CCCs) and phosphate conversion coatings (PCCs), otherwise suffering from escalating stringency of environmental and health regulations [17,18].

## 2. Experimental

### 2.1. Materials

Aluminium alloy EN AW-5754 (denoted as AA5754) in the form of a 1.5 mm thick panel was supplied by Impol 2000 d.d., Slovenska Bistrica, Slovenia. The following chemical composition was specified by the manufacturer: Mg 2.6–3.6 wt%, Mn 0–0.5 wt%, Si 0–0.4 wt%, Fe 0–0.4 wt%, Cr 0–0.3 wt%, Zn 0–0.2 wt%, Ti 0–0.15 wt%, Cu 0–0.1 wt%, Al reminder.

Original panels were cut into smaller square sheet specimens measuring 2.5 cm × 3.5 cm, each featuring punched 3 mm diameter holes for convenient immersion into $H_2ZrF_6$ conversion baths. For surface analysis, samples were further cut out to sizes of up to 1 $cm^2$.

### 2.2. Chemicals

The solutions used in this study were made using analytical reagent grade chemicals in their as-received state: absolute ethanol (EtOH, Merck KGaA, Darmstadt, Germany), NaCl (Fisher Scientific, Leicestershire, UK), $(NH_4)_2SO_4$ (Acros Organics Geel, Belgium), $NH_4HCO_3$ (Sigma-Aldrich, Steinheim, Germany), $H_2ZrF_6$ (50 wt% in water, Sigma-Aldrich, Saint Louis, USA), $CuSO_4 \times 5\,H_2O$ (Sigma-Aldrich, Saint Louis, USA), HCl (37 %, VWR International S.A.S, Fontenay-sous-Bois, France) $Pb(CH_3COO)_2 \times 3\,H_2O$ (Sigma-Aldrich, Saint Louis, USA). For chemical pretreatments, SurTec®'s chemical products (SurTec International GmbH, Bensheim, Germany), supplied by SurTec Adria, d.o.o. (Ljubljana, Slovenia) were used: SurTec® 089, SurTec® 132, SurTec® 141 and SurTec® 496. SurTec® 089 is a detergent booster concentrated liquid product containing non-ionic surfactant alcohols in ethoxylated forms of amines, alkyls and fatty alcohols. SurTec® 132 is a slightly alkaline builder, free of silicates and surfactants, containing tetrapotassium pyrophosphate. SurTec® 141 is an alkaline builder, free of surfactants, containing phosphates, sodium tetraborate and silicates. SurTec® 496 is a high-end desmutting concentrated liquid product containing sulfuric acid, iron(III) salts, nitric acid and hydrofluoric acid.

The solutions were prepared utilising Milli-Q Direct water from Millipore in Billerica, Massachusetts, USA, characterised by a resistivity $\geq$ 18.2 MΩ cm at 25 °C. Water with a total organic carbon (TOC) value below 5 ppb was employed for both rinsing samples and preparing solutions.

### 2.3. Samples and solutions preparation

#### 2.3.1. Grinding

The initial step in sample preparation involved manual wet-grinding using SiC papers up to P4000 grit on a LaboPol-5 grinding/polishing machine operating at 300 rpm (Struers, Ballerup, Denmark). The decision to grind up to a P4000 grit was made to ensure appropriate roughness ($R_a \approx$ 20–30 nm) for applying nanometric ZrCC coatings, given that the resulting roughness is established to be within the nanometric range. Following the grinding process, the samples underwent a 5-minute ultrasonication in absolute ethanol using a 37 kHz, 100 % power Elmasonic P ultrasonic bath for cleaning. Subsequently, the samples were rinsed with absolute ethanol and Milli-Q water before being dried using compressed $N_2$.

#### 2.3.2. Chemical pretreatment

Before conversion, chemical pretreatment was carried out using alkaline cleaning and desmutting. The specimens were immersed in the respective SurTec® solutions on a C-MAG HS 7 magnetic hotplate stirrer (IKA®-Werke GmbH & Co. KG, Staufen, Germany). The stirring rate was set at 150 rpm, and the temperature was maintained at 60 °C, except for the desmutting step, which was conducted at room temperature. The procedure following the laboratory-adapted recommendations provided by SurTec for aluminium alloys was used: a 10 min alkaline cleaning in 3 vol% (30 mL/L) SurTec® 132 + 0.5 vol% (5 mL/L) SurTec® 089, pH= 7.4, followed by a 3 min acid desmutting in 20 vol% (200 mL/L) SurTec® 496, pH= 0.3. Glass beakers with a volume of 500 mL were employed for rinsing step.

Following each alkaline cleaning/desmutting step, a thorough double rinse with Milli-Q Direct water was conducted through two distinct steps: (i) an approximately 30-second vigorous circular rinse using a wash bottle on both sides of the sample, and (ii) a 1-minute immersion in a clean Milli-Q Direct water bath. Given the heightened sensitivity of

ZrCCs to alkaline contamination, a minimum of two rinses is mandated between the cleaning and coating stages [19]. The primary objective of the chemical pretreatment step was not only to eliminate impurities but also to establish a hydrophilic surface conducive to successful zirconium conversion [20]. A simple "water-break test" served as an indicator of effective surface cleaning, wherein the rinse water uniformly coated the entire sample surface after cleaning [21,22].

#### 2.3.3. Conversion treatment

Immediately after the chemical pretreatment, the samples, which retained a fully wet surface, were submerged into $H_2ZrF_6$ conversion baths. These baths featured various combinations of factor settings pre-established by the selected RSM design (*vide infra*).

As the precipitation of zirconia from $H_2ZrF_6$ tends to occur at a relatively low pH range of 3–5 [3,8], the $H_2ZrF_6$ solutions were prepared by initially diluting a 50 wt% $H_2ZrF_6$ solution in a small volume of water. The solution was then filled up to the final volume, with the pH adjusted under vigorous stirring using a diluted (15 wt%) $NH_4HCO_3$ solution, which also serves as a buffer to extend the lifespan of the prepared baths [21]. The pH was monitored using a pH meter 827 pH-lab connected to a Solitrode HF combined pH electrode suitable for measurements in HF and $F^-$-containing solutions (Metrohm AG, Herisau, Switzerland).

Conversion baths were set up in Teflon beakers (V = 250 mL). Samples were immersed in these baths and suspended from a plastic stick. The prepared $H_2ZrF_6$ solutions were stored in polyethylene bottles due to the release of HF with increased pH [3]. Samples were gently moved back and forth through the conversion bath intermittently to allow fresh solution access to the surface, a practice occasionally observed in industrial settings with manual immersion.

After the conversion process, the samples were rinsed in two stages: (i) a vigorous circular rinse on both sides using a wash bottle for approximately 30 seconds, and (ii) a 1-minute dip in a clean Milli-Q Direct water bath. The samples were then dried with a stream of compressed $N_2$ from bottom to top, followed by an additional 10 minutes of drying on a C-MAG HP 4 hotplate (IKA®-Werke GmbH & Co. KG, Staufen, Germany) at 80 °C, following common industrial practices. Additionally, one set of AA5754 samples designated for drop tests and electrochemical measurements was left to air-dry for 24 hours to assess the influence of drying on the results.

### 2.4. Response surface methodology

After an extensive review of the existing literature, we explored a range of $H_2ZrF_6$ concentrations from 150 to 1500 ppm, pH levels from 3 to 5, and conversion durations from 60 to 900 seconds. These parameters mirror those employed in our previous work [1].

The exploration of this range through a central composite design (CCD) within the framework of response surface methodology (RSM) led to the variation of all factors at five levels (Table 1, Fig. S4): concentration was varied at 150, 424, 825, 1226 and 1500 ppm, pH was varied at 3.0, 3.4, 4.0, 4.6 and 5.0 and conversion time was varied at 60, 230, 480, 730 and 900 s. Only the centre point (825 ppm/480 s/pH 4.0) was sextuplicated, according to the postulation of RSM. In contrast to previous work [1], where such a wide parameter range led to identifying the best-performing regions, the experimental design in the case of AA5754 required two extensions with additional runs (Table 2). Narrowing down a part of the experimental space that indicated the best conditions, namely concentration variations at 150, 656 and 825 ppm, pH values at 3.4, 4.0 and 4.3 and conversion times at 355, 418 and 480 s, resulted in a D-optimal experimental design.

The main text includes only the RSM plots after the last augmentation focused on the concentration region 150−825 ppm, pH 4−4.6 and conversion time between 230−480 s. Tabular RSM results, along with all additional information necessary for understanding the execution of RSM in this work, including augmentations, ANOVA (analysis of variance) test results, and model adjustments for each RSM response, are provided in the Supplementary material, Sections 2 and 3. RSM was performed via Design-Expert software version 13 (Stat-ease, Inc., Minneapolis, MN, USA).

To assess the sensitivity and feasibility of observing the effects of conversion bath parameters, corrosion resistances of ZrCC-coated AA5754 samples assessed by non-electrochemical and electrochemical methods were selected as RSM responses. For clarity and ease of comprehension, a flowchart detailing sample preparation, measurements, and important factors considered is provided in Fig. S1.

#### 2.4.1. Non-electrochemical measurements

Initially, a direct and non-electrochemical method called the drop test was employed. This method involves measuring the time in seconds required for the coating to completely dissolve, as indicated by a colour change signifying that the reduced reagent cations have reached the bare metal surface. For AA5754, "Akimov's reagent" [15] was utilised (82 g/L $CuSO_4{\cdot}5\,H_2O$, 33 g/L NaCl, and 13 mL/L of 0.1 N HCl, pH=3.6). The time required for colour was measured using a stopwatch. The response obtained from this approach is denoted as the "protective ability" (PA); the longer the time for colour change, the better the PA. PA measurements were performed after a 10-minute conversion and 10-minute drying period at 80 °C and after 24 hours of air drying. Notably, determining the exact endpoint of the colour change with this method was somewhat subjective, with timing variations of a few seconds. However, the method remains effective for detecting changes when the time difference is above 10 seconds. A representative example is given in the video in the Supplementary material.

#### 2.4.2. Electrochemical measurements

Electrochemical experiments were conducted utilising a Multi Autolab/M204 potentiostat/galvanostat from Metrohm Autolab, Utrecht, Netherlands, controlled by Nova 2.1 software. Measurements were carried out in custom-made "clamp-on" electrochemical cells (250 mL) designed for flat, thin-coated samples with reduced susceptibility to crevice corrosion [23]. The cell components were specially fabricated and assembled by bonding with the strong 1-component solvent adhesive ACRIFIX® 1S 0116 (Evonik Performance Materials GmbH, Darmstadt, Germany).

The electrochemical setup comprised a three-compartment system: the sample served as the working electrode (WE), attached at the bottom by pressing against an o-ring to facilitate the escape of gas bubbles generated during cathodic reactions, thereby minimising the risk of crevice corrosion. A carbon rod acted as the counter electrode (CE), and a saturated Ag/AgCl (3 M) electrode served as the reference electrode (RE) at $E = 0.297$ V vs. the standard hydrogen electrode, positioned near the WE to reduce uncompensated IR drop. All potentials are referenced to the Ag/AgCl (3 M) scale. The working electrode's area was 0.785 $cm^2$, and measurements were conducted under ambient conditions.

Before electrochemical measurements, samples were allowed to rest

**Table 1**
Summary of central composite design (CCD) before augmentation.

| Factor | Name | Units | Type | SubType | Min. | Max. | Coded Low | Coded High | Mean | Std. Dev. |
|---|---|---|---|---|---|---|---|---|---|---|
| A | pH | | Numeric | Continuous | 3.00 | 5.00 | −1 ↔ 4.00 | +1 ↔ 4.59 | 4.08 | 0.4582 |
| B | t | s | Numeric | Continuous | 60.00 | 900.00 | −1 ↔ 230.27 | +1 ↔ 480.00 | 439.03 | 194.78 |
| C | c | ppm | Numeric | Continuous | 150.00 | 1500.00 | −1 ↔ 150.00 | +1 ↔ 825.00 | 693.16 | 377.00 |

**Table 2**
Summary of central composite design (CCD) after the second augmentation.

| Factor | Name | Units | Type | SubType | Min. | Max. | Coded Low | Coded High | Mean | Std. Dev. |
|---|---|---|---|---|---|---|---|---|---|---|
| A | pH | | Numeric | Continuous | 3.41 | 4.59 | −1 ↔ 4.00 | +1 ↔ 4.59 | 4.08 | 0.4582 |
| B | t | s | Numeric | Continuous | 230.27 | 480.00 | −1 ↔ 230.27 | +1 ↔ 480.00 | 439.03 | 194.78 |
| C | c | ppm | Numeric | Continuous | 150.00 | 825.00 | −1 ↔ 150.00 | +1 ↔ 825.00 | 693.16 | 377.00 |

at the open circuit potential (OCP) and monitored until reaching a quasi-stable state, usually after 1 hour [24]. Subsequently, electrochemical impedance spectra and potentiodynamic polarisation curves were measured. This choice was made to avoid electrode alteration due to an excessively high amplitude used in EIS for this case.

EIS measurements were taken at the OCP with a perturbation potential amplitude of ± 10 mV (root mean square). A series of 51 logarithmically spaced frequencies were applied over 7 decades, spanning from 100 kHz to 10 mHz. The NOVA 2.1 software was employed to fit the EIS data to the equivalent circuit model using the Levenberg-Marquardt optimisation algorithm.

PPC measurements were carried out in the potential range from −150 mV vs. OCP to 1 V vs. the reference electrode in the anodic direction until the current reached 1 mA or 1 V, with a scan rate of 1 mV $s^{-1}$. The Tafel extrapolation method was used to extract corrosion parameters (corrosion potential, $E_{corr}$, and corrosion current density, $j_{corr}$) from PPCs, and polarisation resistance ($R_p$) was calculated according to the ASTM G59–97 standard [25] using Nova 2.1 software. The assessment was conducted according to the rule [24], which specifies that the linear Tafel region should span at least one order of magnitude in current density and preferably two decades for more accurate extrapolation [24]. In most cases, we could use one decade on the cathodic branch and two, but often three, on the anodic branch.

The electrolyte used in the study was a dilute Harrison's solution (3.5 g/L $(NH_4)_2SO_4$ and 0.5 g/L NaCl, pH = 5.2), commonly employed for simulating atmospheric conditions and striking a balance between solution corrosivity and the ability to rank corrosion properties among different ZrCCs.

Various electrochemical responses were employed in RSM: $R_p$ was evaluated using both EIS and PPC, whereas $j_{corr}$ was derived from PPCs. The criteria for selecting best-performing preparation conditions were based on maximal $R_p$ and minimal $j_{corr}$.

*2.4.2.1. EIS experimental details.* EIS experimental details are elaborated in the previous article [1]. Similar to prior work [1], the analysis of EIS spectra from a larger sample set is leveraged to reveal various time constants. Additionally, the choice of the equivalent electrical circuit (EECs) is based on a prior understanding of substrate and ZrCC behaviour in NaCl-containing solutions, comparing specific time constants' presence/absence relative to bare substrates.

Post-EIS measurements, samples were examined for stability, causality, and linearity by analysing raw AC potential and current data through Kramer-Kronig's test, Lissajous, and AC current / AC potential resolution plot [26] (not shown). NOVA software, equipped with accessible raw EIS data analysis tools, was employed for this purpose.

The suggested EECs for fitting EIS spectra incorporate the minimum essential elements for interpreting the data (inset in Fig. 2a), adhering to Occam's razor principle [26]. The focus was on attaining a predictive model that captures significant electrochemical processes rather than an overly complex fitting model. While the proposed models are tentative, they have proven valuable in interpreting the impact of conversion bath parameters. The number of time constants was determined based on a visual examination of Nyquist and Bode plots, ensuring symmetry in phase angle peaks and capacitive arcs and analysing fit residual errors. Periodicity in residual error analysis indicated the potential omission of certain time constants [27]. In particular, while the symmetry of phase angle in Bode plots for ZrCC-free samples and the analysis of residual errors suggest the inclusion of additional time constants, likely corresponding to aluminium oxide and charge transfer at the electrolyte/metal interface, we employed a single time constant to fit all EIS spectra of AA5754 incorporated into a simple Randels circuit ([R1 (R2CPE1)]). Here, R1 represents the electrolyte resistance, R2 accounts for defects formed during exposure, and CPE1 represents the interfacial capacitance where these reactions occur. Presumably, contributions from pore impedance and charge transfer resistance are summed within $R_p$, simplifying the system to R1+R2 +R3 + ⋯+Rn= $R_p$. This choice still maintained the significantly improved $R_p$ values in ZrCC-free samples. Constant phase element (CPE) instead of capacitor (C) was employed to compensate for the distribution of relaxation times caused by surface inhomogeneities [28].

### 2.5. Surface analysis

Surface analysis was conducted using scanning electron microscopy (SEM) combined with energy-dispersive X-ray spectroscopy (EDS). After grinding AA5754 samples up to 4000 grit, an additional polishing step was carried out using a 1 μM diamond suspension Dia-Duo 2 on an MD-Nap polishing cloth (Struers, Ballerup, Denmark). The polishing was followed by cleaning and conversion steps in Petri dishes with non-stirred solutions, chosen due to the smaller sample size than those used for non-electrochemical and electrochemical measurements. Afterwards, samples were allowed to air-dry for 24 hours.

SEM analyses were conducted using a field emission SEM JSM 7600 F, JEOL, Japan, equipped with EDS (Inca Oxford 350 EDS SDD). SEM images were captured in secondary electron (SE) and back-scattered modes, employing a concentric back-scatter (CBS) detector. Beam voltages of 5 kV and 15 kV were applied, with the latter chosen for its higher penetration depth, specifically to detect intermetallic particles in AA5754. Before analysis, the samples were coated with a thin carbon layer to mitigate the charging effect.

## 3. Results and discussion

### 3.1. Electrochemical results

In the main text, plots of discussion-relevant electrochemical results are separated from those that present the electrochemical results for the coatings prepared using all conversion bath parameters used in RSM (Table 1). Tabular electrochemical results are presented in Supplementary material, Section 1.

#### 3.1.1. Potentiodynamic polarisation curves

A consistent cathodic shift is generally observed across all AA5754-ZrCC-treated samples (Fig. 1a-c, Table S1) - except for the sample ZrCC deposited at 825 ppm/60 s/pH 4. This shift is accompanied by an extension of the passive region within the ZrCCs, especially for samples 150 ppm/230 s/pH 4.6 and 150 ppm/480 s/pH 4.6, the latter showing a slightly more extended prolongation as compared to ZrCC-free samples. Conversely, for the alkaline-cleaned and alkaline-cleaned and desmutted samples, an anodic shift is noticeable, alongside a reduction in $j_{corr}$. However, for the alkaline-cleaned and desmutted sample, a pitting onset occurred at a significantly more negative potential compared to the alkaline-cleaned sample. The $j_{corr}$ of ZrCC-treated samples exhibit minimal divergence. Nevertheless, it is worth noting that the samples 825 ppm/480 s/pH 3.0 and 825 ppm/480 s/pH 4.0 stand out, suggesting a potential adverse impact of lower pH and higher concentrations, for the

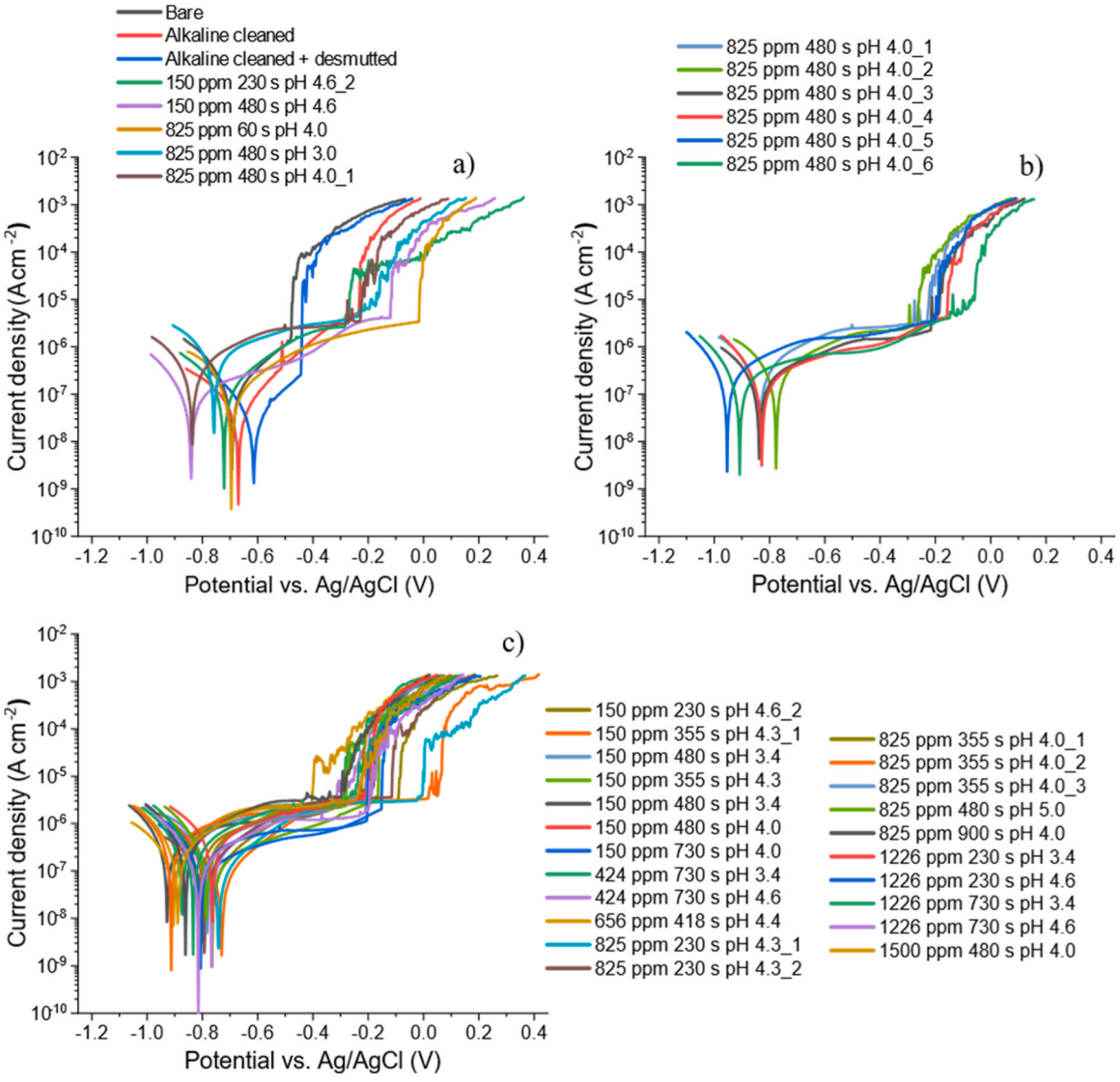


**Fig. 1.** Potentiodynamic polarisation curves in dilute Harrison's solution recorded for AA5574: a) chosen results for discussion, b) results of central point repetitions, and c) results obtained under the remaining conditions. $dE/dt = 1$ mV/s. Rest periods at OCP were 1 h. A clearer presentation of the PPC curves, separated into additional graphs for better distinction from Fig. 1c, is available in Supplementary material, Fig. S2.

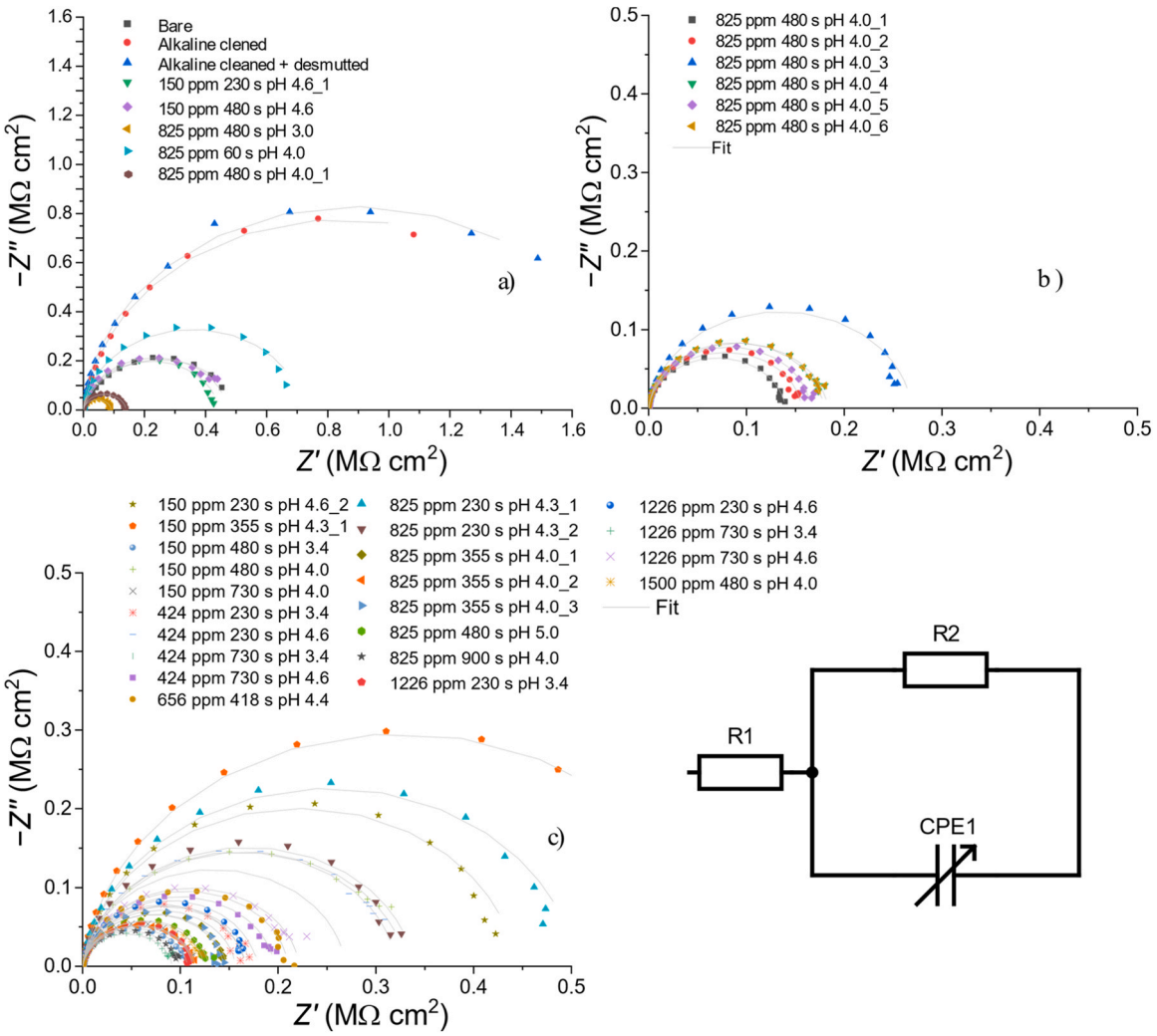


**Fig. 2.** EIS results (Nyquist plots) in dilute Harrison's solution for AA5574: a) chosen results for discussion with an inset of EEC used for EIS fitting of all samples, b) results of central point repetitions, c) results obtained under the remaining conditions. A clearer presentation of the EIS spectra, separated into additional graphs for better distinction from Fig. 2c, is available in Supplementary material, Fig. S3.

latter, particularly within the middle to higher pH range. Thus, these findings permit the implementation of electrochemical parameters deduced for PPCs as responses for RSM. However, it is necessary to employ ANOVA in RSM to identify significant differences (Supplementary material, Section 3).

### 3.1.2. *Electrochemical impedance spectroscopy data*

Transmission electron microscopy analysis at the cross-section of Šekularac et al. [10], confronted with the barrier layer theory of MacDonald [29], showed a tri-layer (the bottom and middle that cannot be easily distinguished and a distinguished top layer) structure of ZrCC on an AA3003 alloy which preserved overall thickness during a 5-day immersion in 0.5 M NaCl. However, the bottom layer thickened due to the incorporation of substrate and substrate alloying element corrosion products. The top (outer) layer preserved the Zr content with exchanged $F^-$ with $Cl^-$ ions from the solution. However, the middle layer, consisting mainly of $ZrO_2$, experienced the least alteration. This contrasts CCCs [11], which contain chromate corrosion products and a porous CCC layer separated from the substrate by a dense barrier layer [29]. Zr in ZrCC does not change its valency state, unlike Cr, meaning that the corrosion products formed only pertain to the underlying substrate.

One time constant is observed in all Nyquist plots for ZrCC-AA5754 (Fig. 2, Table S2). However, in all cases, significantly smaller capacitive arcs in the Nyquist plot obtained for ZrCC-coated samples than ZrCC-free samples do not favour the higher corrosion protection offered by ZrCCs, as would be concluded based on PPC results (Fig. 1).

The reason for this will be explained in the section below on SEM micrographs (see below Figs. 5–6), which show cracking of remarkably thicker ZrCCs on Al-Fe intermetallic particles (IMPs). According to the results, the best-performing samples are at low concentration (150 ppm), low to middle conversion time (230–480 s) and higher pH (4.6), which approached the corrosion resistance of the bare sample. In addition, corrosion resistivity among ZrCC-free samples follows the sequence alkaline-cleaned + desmutted > alkaline-cleaned > bare.

Owing to the same low-frequency limit applied in measurements (0.01 Hz), the EEC employed herein is similar to one used by Buchheit et al. [30] with only a one-time constant (R2-CPE1), i.e. EEC from Fig. 2a). It should be noted that the inductive behaviour at low frequencies observed in the Nyquist spectra (Fig. 2), was without any discernible pattern. Moreover, this inductive behaviour was not associated with pitting, as confirmed by visual analysis (not shown). Instead, it appears to be caused by surface roughness, adsorption effects, or ion exchange from the solution [31,32] (potentially involving $Cl^-$ and $F^-$, as shown by the XPS study by Šekularac et al. [11]).

## 3.2. *RSM results*

As pointed out in our previous work [1], thin film results, typically

within a similar range, may yield statistically unreliable data. A larger sample size, such as in RSM, is crucial when the effect size is too small for statistical significance, enhancing the test's power for detecting significant differences [5–7,33]. The ZrCC results of interest are contrasted with both bare and chemically pretreated samples, collectively referred to as "ZrCC-free" samples.

#### 3.2.1. RSM for protective ability

Based on ANOVA analysis (the Supplementary material, Section 3), it can be inferred that the model is significant; however, the lack-of-fit is also significant.[2] Based on p- and F-values, the two most significant model terms for **PA after 10 minutes** are linear terms of conversion time and concentration. However, the significant lack-of-fit, despite sufficient $R^2$ and adequate precision values, indicates that the model is unreliable. The response surface in Fig. 3a is presented herein as it depicts the obtained data but cannot be used for characterisation or optimisation.[3] However, from (Fig. 3a and Table S3), it can be observed that PA values are higher at lower concentrations of 150 ppm than at 825 ppm.

On the other hand, based on ANOVA analysis in the Supplementary material, Section 3, it can be inferred that the model for the **PA after 24 hours** is significant, with the lack-of-fit being insignificant.

The response surface equation in terms of actual factors for PA after 24 h is given in Eq. 1:

$$1 / (\text{Sqrt (PA after 24h)}) = 0.093508 + 0.000089 \times t + 0.000054 \times \gamma \quad (1)$$

Similarly, based on p- and F-values, the two most significant model terms for PA after 24 hours are linear terms of conversion time and concentration. $R^2$ and adequate precision values confirm that the model is reliable enough to characterise the process.

Eq. 1 translates to RSM plot in Fig. 3b showing a marked enhancement after 24 hours for all samples, although with reduced predictive variability at higher concentrations compared to the 10-minute timeframe (Fig. 3a). This phenomenon is likely due to the development of a more densely packed film formed upon exposure to air, potentially involving the growth of a native alumina film within developed pores/cracks, taking into account the Pilling-Bedworth ratio, as shown in [1]. Drop test results of ZrCC-free samples also follow that trend, with alkaline cleaned + desmutted sample showing the highest PA value (52 s) (Table S3).

However, the pH does not emerge as a significant, i.e. influential factor in determining PA within both timeframes, evidenced by a lack of curvature and ANOVA analysis in the Supplementary material, Section 3. Moreover, while the RSM plots do not attain an optimal point, they serve as valuable guides for narrowing the experimental space down to lower concentrations and shorter conversion times.

In summary, based on drop test results, AA5754 shows better protective ability with prolonged drying at lower concentrations and shorter conversion times, with pH not being a significant influencing factor.

#### 3.2.2. RSM for corrosion current density

Based on ANOVA analysis (see the Supplementary material, Section 3), it can be inferred that the model for $j_{corr}$ is significant, with the lack-of-fit being insignificant, although with a relatively low probability. Furthermore, based on F-values, the two most significant model terms are the linear terms of conversion time and the interaction term of conversion time and concentration. However, relatively low $R^2$, regardless of sufficient adequate precision values, suggest the model is not reliable. These results imply that $j_{corr}$ might not be the most appropriate parameter for evaluating ZrCC performance, even though it accurately depicts the obtained data.

#### 3.2.3. RSM for polarisation resistance from Tafel extrapolation

Based on ANOVA analysis in the Supplementary material, Section 3, it can be inferred that the model for $R_p$ from Tafel extrapolation is significant, with the lack-of-fit being insignificant. All three factors were found to have an effect, either the main or interaction, as shown in Eq. 3; however, based on F-values, the two most significant model terms are the interaction term between conversion time and concentration and linear term of concentration. Moderately high $R^2$ and adequate precision values suggest the model is reliable enough to characterise the process.

The response surface equation in terms of actual factors for $R_p$ Tafel extrapolation on AA5754 is given in Eq. 2:

$$1 / (\text{Sqrt}(R_p \text{ Tafel extrapolation})) = 0.010104 - 0.001627 \times \text{pH} - 4.93342\times 10^{-6} \times t - 0.000018 \times \gamma + 3.50121\times 10^{-6} \times \text{pH} \times \gamma + 1.00561\times 10^{-8} \times t \times \gamma \quad (2)$$

Eq. 2 translates to RSM plots in Fig. 4a,b and Table S3, where the best-performing region for $R_p$ obtained through Tafel extrapolation of PPCs is predicted at higher pH levels (4.3–4.6), with a low concentration (150 ppm) and a conversion time (480 s). This starkly contrasts with higher concentrations (825 ppm), where a marginal increase in $R_p$ is observed at shorter conversion times (230 s) and lower pH values (4.0).

#### 3.2.4. RSM for EIS results

Based on ANOVA analysis in the Supplementary material, Section 3, it can be inferred that the model for $R_p$ from EIS is significant, with the lack-of-fit being insignificant. All three factors were found to have an effect, either the main or interaction, as shown in Eq. 3; however, based on F-values, similar to $R_p$ from Tafel extrapolation, the two most significant model terms are the interaction term between conversion time and concentration and linear term of concentration. Moderately high $R^2$ and adequate precision values suggest the model is reliable enough to characterise the process.

The response surface equation in terms of actual factors for $R_p$ Tafel extrapolation on AA5754 is given in Eq. 2:

$$1 / (\text{Sqrt } (R_p \text{ EIS})) = 0.012297 - 0.001988 \times \text{pH} - 6.05195\times 10^{-6} \times t - 0.000022 \times \gamma + 4.36398\times 10^{-6} \times \text{pH} \times \gamma + 1.17673\times 10^{-8} \times t \times \gamma \quad (3)$$

Eq. 2 translates to RSM plots in Fig. 4c,d and Table S3 that closely resemble the $R_p$ from Tafel extrapolation (Fig. 4a,b), indicating a strong correlation. Specifically, the best-performing conditions are once again projected at higher pH levels (4.3–4.6), accompanied by a low concentration (150 ppm) and a medium conversion time (480 s).

#### 3.2.5. Comments on the overall feasibility of RSM models for AA5754

RSM results for AA5754 are summarised in Table 3 (for complete

[2] The F-value in an ANOVA is calculated as: variation between sample means divided by variation within the samples. The higher the F-value, the higher the variation between sample means relative to the variation within the samples. The coefficient of determination ($R^2$) is a number between 0 and 1 that measures how well a statistical model predicts an outcome. In RSM, centre points are typically the only repeated runs. They are particularly useful because the optimal response is often expected near the centre of the design space, enhancing prediction accuracy in that region. However, replication is not restricted to the centre—experiments can be repeated in other areas if greater precision is required. Regardless of location, replication allows for estimating pure error, which represents the system's natural variability under identical conditions. This pure error is essential for the lack-of-fit test, which evaluates whether the model adequately describes the data. The lack-of-fit test compares the variation unexplained by the model to pure error. If the lack-of-fit F-value is not significant, it suggests the model fits well, meaning deviations from predictions are likely due to random noise rather than systematic errors. In other words, the differences between predicted and actual values stem from random fluctuations rather than model inadequacy, indicating a good fit.

[3] Points above the design indicate measured values exceeding the predicted surface, while points below the design indicate those below, reflecting a difference between predicted and actual observations.

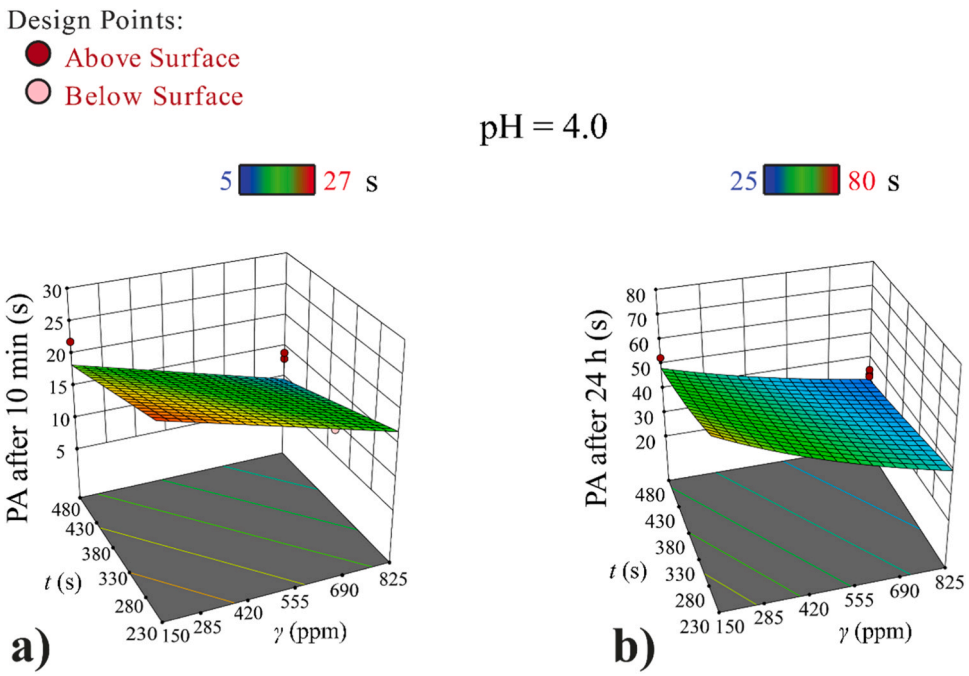


**Fig. 3.** RSM plots for AA5754 (after the second augmentation) for different responses: (a) PA after 10 min, (b) PA after 24 h at pH = 4.0. The extent of results is represented on colour scales above the graphs. Measured points denoted by red and pink circles are located above or below predicted values, respectively.

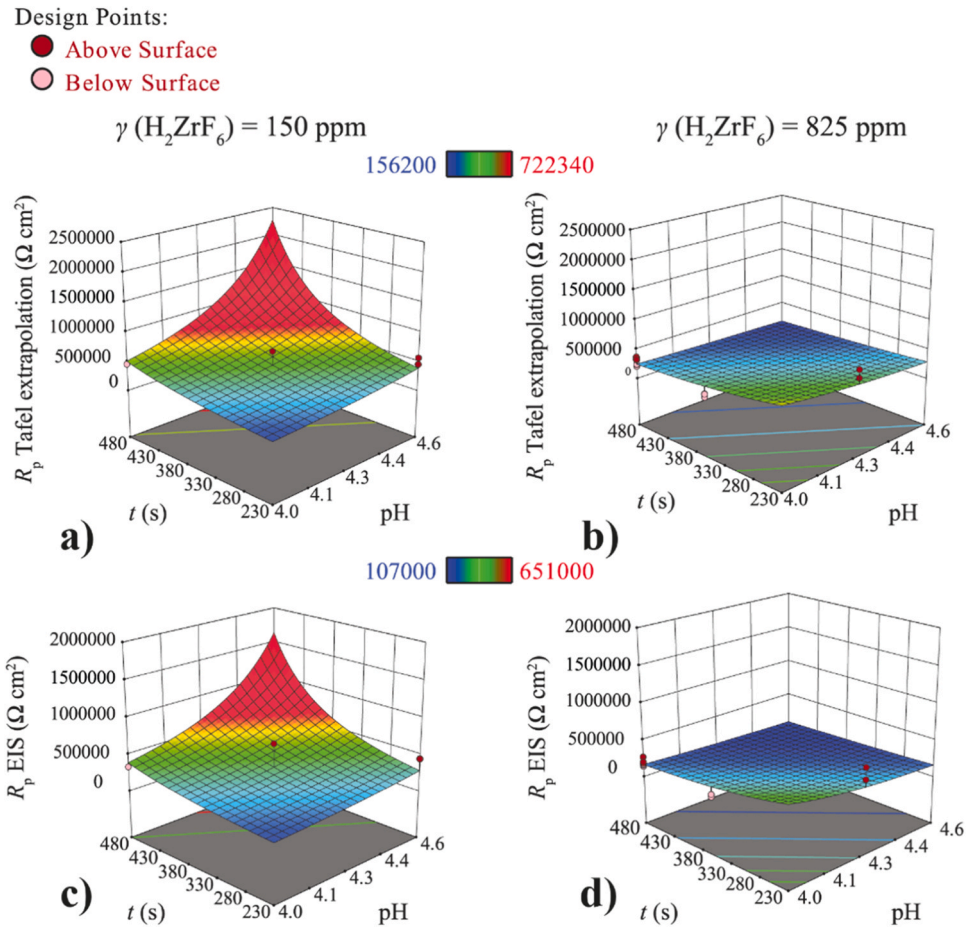


**Fig. 4.** RSM plots for AA5754 (after the second augmentation) for different responses: (a-b) $R_p$ Tafel and (c-d) $R_p$ EIS for concentrations $\gamma(H_2ZrF_6)$ of 150 and 825 ppm. The extent of results is represented on colour scales above the graphs. Measured points denoted by red and pink circles are located above or below predicted values, respectively.

**Table 3**
Comparison of the feasibility of each technique and its responses for evaluating ZrCCs based on RSM model analysis. Combined with results for CRS and Zn from [1].

| Technique | | Protective ability | | Potentiodynamic polarisation curves | | Electrochemical impedance spectroscopy |
|---|---|---|---|---|---|---|
| **CRS** | Response | PA after 10 min | PA after air-drying for 24 h | not considered | | $R_p$ |
| | Applicability | characterisation | not considered | | | characterisation, optimisation |
| **Zn** | Response | PA after 10 min | PA after air-drying for 24 h | $j_{corr}$ | $R_p$ | $\|Z\|$ at 0.25119 Hz |
| | Applicability | / | characterisation, optimisation | characterisation | / | characterisation, optimisation |
| **AA5754** | Response | PA after 10 min | PA after air-drying for 24 h | $j_{corr}$ | $R_p$ | $\|Z\|$ at 0.25119 Hz |
| | Applicability | characterisation | characterisation, optimisation | / | characterisation | characterisation, optimisation |

results, please see Supplementary material, Section 3). The PA after 10 minutes can be used only for characterisation, making less physical sense than after 24 hours, which is more convenient for characterization and optimisation. The $j_{corr}$ model is the least suitable, while the $R_p$ from Tafel extrapolation is better for characterisation. Once again, as shown in our previous work [1], $R_p$ from EIS remains the most suitable for both characterisation and potential optimisation, as it shows the lowest discrepancy in criteria for the difference between predicted and adjusted $R^2$ compared to other electrochemical responses.

### 3.3. Surface analysis by SEM/EDS

Following developing an empirical model through RSM and estimating the main and potential interaction effects of specific factors, an SEM analysis was conducted on the most scientifically interesting samples to support and substantiate the observed RSM response results.

Only the Zr, O and Al contents obtained through EDS were deemed relevant for discussion. The atomic percentages of these elements, along with the locations where EDS spectra were acquired on SEM micrographs, are depicted in Figs. 5–6. Comprehensive EDS analyses can be found in Supplementary material, Section 4 (Figs. S7-S8). The coating density significantly impacts the depth of electron penetration. The density may be noticeably reduced in practical scenarios, leading to a faster beam arrival at the substrate. Our Monte Carlo simulations (not shown) reveal that on the AA5754 matrix, the penetration depth is 60 nm at 3 kV, 230 nm at 5 kV, and 1560 nm at 15 kV, assuming a model thickness of 20 nm. Additionally, for AA5754 IMPs, the penetration depth is 70 nm at 3 kV, 130 nm at 5 kV, and 950 nm at 15 kV, using a model thickness of 1000 nm.

Given that the penetration depth presumably exceeds the coating thickness (typically ranging from 10 to 70 nm on all substrates, excluding IMPs [8]) for AA5754 IMPs, 15 kV is sufficient to detect the IMPs. However, it is likely not adequate to grasp its thickness fully under various ZrCC parameter settings. Furthermore, considering peak overlapping, especially that of F and Fe [34], assessing the quantitative impact of concentration and conversion time on ZrCC thickness is unreliable [35,36]. Nevertheless, both thickness and coating density can be indirectly inferred.[4]

AA5754 alloy contains $(MnFe)Al_6$, $\alpha$-$(MnFe)_3SiAl_{12}$, [37] $AlFe_3$, $Mg_2Si$ and, sporadically, $Al_6CuMg_4$ IMPs [38]. High Fe:Mn ratios observed from EDS spectra on bare and chemically pretreated samples (Fig. S8) are common for AA5754, where a significant portion of Mn is substituted by Fe. The semi-quantitative nature of EDS and the strong influence of matrix signal at 15 kV [35] do not allow for identification of the exact type of IMPs except that the main ones found to be important for conversion are Fe-containing and are referred to as Al-Fe IMPs. However, understanding the behaviour of aluminium's IMPs at different pHs is still under research and can differ greatly for the same IMPs in different aluminium alloys in the same series [39–42]. Nevertheless, Fe exhibited cathodic behaviour in all Fe-containing IMPs, which is needed for further discussion [43,44]. Therefore, the general knowledge of Fe's behaviour can be applied to Al-Fe IMPs to explain ZrCC formation on AA5754.

In contrast to bare, chemically pretreated samples have significantly increased Fe content on Al-Fe IMPS (Fig. S7), pointing to a possible enrichment due to the selective dissolution of Mg [45]. In addition, after desmutting, Al-Fe IMPs exhibited a rather porous structure (Fig. 5). The current study employed a commercial desmutting step that contained $H_2SO_4$, $HNO_3$, and HF. The latter two components were previously studied by Campestrini et al. as an additional pickling step, and their results confirmed that using HF in the desmutting process leads to a severe attack on the Al-matrix, resulting in the better removal of second-phase particles and, possibly, SiC grounding residuals through a drop out [46]. This effect arises as fluorides are well-known for complexing with Al [47–49], further leading to its preferential dissolution across the entire operating range of the conversion bath, as implied by our recent equilibrium calculations [4]. Therefore, lower concentrations of local cathodes on the surface should lead to more uniform alumina formation during the alkaline cleaning and desmutting steps, as well as subsequent more uniform conversion coating deposition. This could explain the superior EIS capacitive loop observed for the desmutted sample as well as improved values of PA compared to bare and alkaline treated samples both after 10 min and 24 h, respectively (Fig. 2). However, although the porosity of structures formed out of IMPs presumably improves their cathodic efficiency, it also makes them more susceptible to pitting corrosion than ZrCC-treated samples, as observed in PPC results (Fig. 1a).

The ultimate confirmation of ZrCC-treated samples' inferior performance in EIS, when compared to ZrCC-free samples, becomes evident in SEM micrographs due to crack formation (Fig. 6). This leads to the EIS response being exclusively governed by charge transfer through substantial defects at the OCP, which are, in fact, larger than the coating thickness (generally around 10–80 nm [8]). In contrast, extended passivation regions in ZrCC-AA5754 samples (Fig. 1) can arise as a direct consequence of pores/cracks being cathodic to the substrate, thereby enabling them to contribute to passivation during the anodic scan in PPC (Fig. 6).

Let us first consider the results at constant pH with increasing concentration and conversion time. The effects of increasing concentration and conversion time at the same pH setting result in thicker coatings on AA5754, just as observed in previous work for Zn and CRS [1], indicated by a higher Zr content on both matrix and IMPs and lower Fe content on IMPs (Fig. S8) (also compare 150 ppm/pH 4.0/480 s (Fig. 6b) and 730 s (Fig. 6d) as well as 825 ppm/ pH 4.0 at 60 and 480 s (Fig. 6f,g). Moreover, the sample 825 ppm/60 s/pH 4.0 (Fig. 6f) confirms that the conversion begins at cathodic sites (Al-Fe IMPs) as indicated by Zr detection only at the IMPs and none at the matrix. Interestingly, in contrast to PA results, electrochemical test results show that 825 ppm/60 s/pH 4.0 offers the same level of corrosion protection as ZrCC-free samples and even a slightly prolonged passivation range (Figs. 1,2). When the coating blocks merely a fraction of the surface, the corrosion rate may stay the same on the remaining bare areas, as the increase in $R_{ct}$ occurs due to a decrease in surface active area. This is already seen in Fig. 1, as this sample is the only one having more

[4] To achieve an accurate evaluation of F content, advanced techniques such as wavelength dispersive X-ray analysis (WDX) with superior energy resolution are necessary to prevent common peak overlap errors encountered in EDS analysis. Consequently, the enclosed EDS micrographs are only semi-quantitative [35,36].

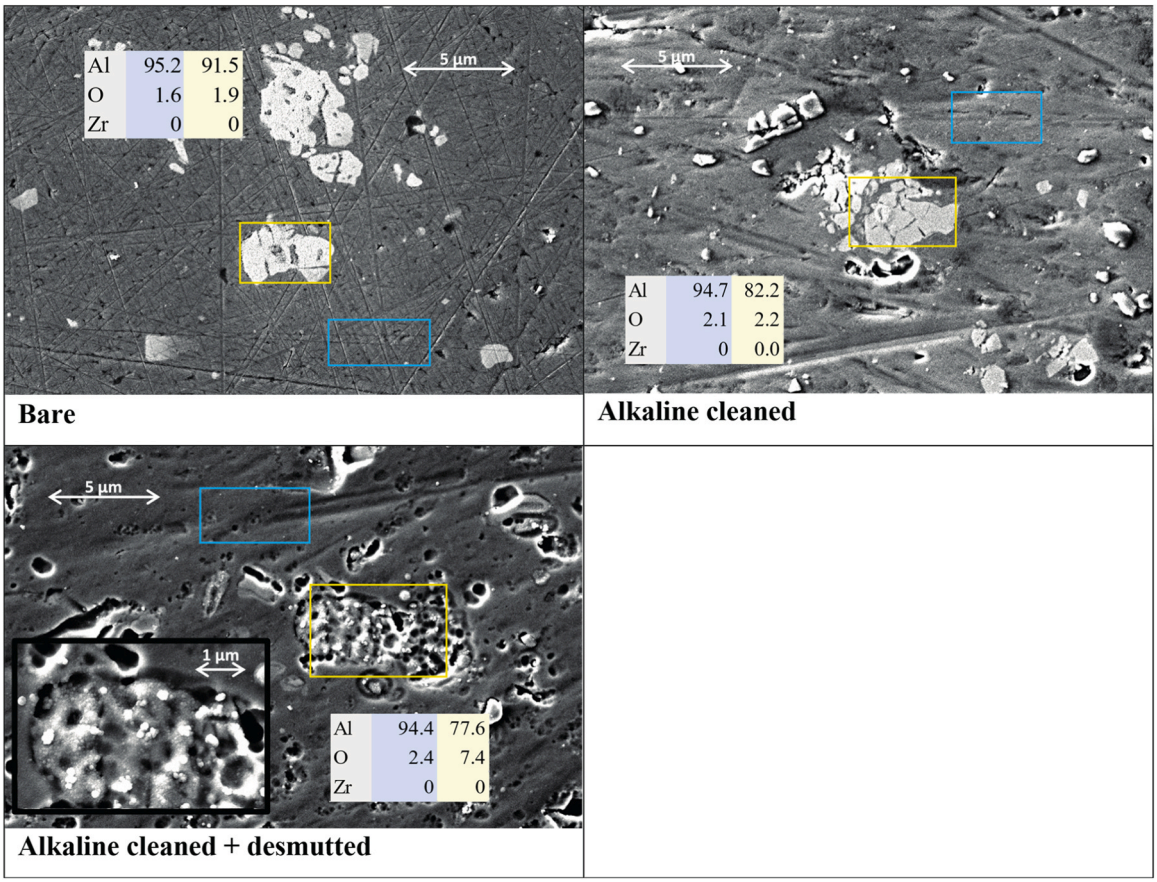


**Fig. 5.** SEM micrographs of bare, alkaline-cleaned and alkaline-cleaned and desmutted AA5754 ZrCC-free samples. The sites of EDS analyses are noted by blue and yellow rectangles, and the results for Al, O and Zr are given in tables (at%). Results for all elements are given in Supplementary material, Section 4). Blue sites belong to the matrix, and yellow sites correspond to intermetallic particles.

negative $E_{corr}$ compared to other ZrCC samples, which is almost the same as the bare sample [50], indicating that more electrochemically active regions are present on the surface [51], and not that the coating provides sufficient protection.

Further increase of conversion time enables ZrCC growth in the lateral direction, aligned with a decreased difference in Volta potential between cathodic IMPs and anodic aluminium matrix [8]. The cathodic reactivity of the IMPs is suppressed after zirconia deposition, lowering the extent of microgalvanic coupling with the matrix, i.e. driving force for ZrCC deposition and allowing for cathodic reactions to continue at Al matrix, along with Al dissolution, similarly to CCCs [52].

In addition, the cathodic action of IMPs is also seen through a higher Zr content obtained at larger IMPs (825 ppm/480 s/pH 4.0 (Fig. 6h)). Concentrations of Zr on IMPs and matrix differ even by order of magnitude, leading to cracking of the coating around the IMPs and enabling ingress of corrosive agents to the substrate. This difference in Zr content is approximately 20 × for samples at 825 ppm and approximately 3–10 × for samples at 150 ppm, except for the sample with pH 3.4, where the difference reaches 20 × , as will be further discussed below.

There is also a significant difference in the morphology of ZrCC at IMPs and matrix, similar to that in CCCs. Compared to small-nodular on the Al-matrix, more compact, thicker and denser zirconia films are formed on the surfaces of IMPs. ZrCCs are cracked around IMPs, owing to a significantly higher deposition rate of ZrCC on IMPs. This behaviour has been shown for ZrCCs throughout the AA series [9]. The fact that the coatings continue to grow on both IMPs and the matrix after a long conversion time results from the permeability of the formed gel and solution access through the cracked IMPs, allowing cathodic reactions to continue [53,54]. Nevertheless, the previously formed particles can also serve as nucleation sites for subsequent precipitation, as proposed in [55].

By comparing Zr contents obtained at low and intermediate concentration settings (150 ppm (Fig. 6a-d) and 825 ppm (Fig. 6e-h)), it can be seen that lower concentration leads to a more uniform coating, reflected in a smaller difference between Zr content on the matrix and IMPs. Prolonging the conversion time at lower concentrations still results in lower Zr content on Fe IMP than shorter conversion times at higher concentrations (compare 150 ppm/730 s/pH 4.0 (Fig. 6d) and 825 ppm/480 s/pH 4.0 (Fig. 6h) and 825 ppm/60 s/pH 4.0 (Fig. 6f) and 150 ppm/480 s/pH 4.0 (Fig. 6b)). This proves that the kinetics of the subsequent conversion film growth is diffusion-controlled, as lower concentrations lead to lower concentration gradients and greater depletion of $H_2ZrF_6$ at the surface. It can be inferred that further growth occurs until the exhaustance of the conversion agent (Zr-bearing component, in this case, $H_2ZrF_6$) and local cathodes near the metal surface, making the process self-limiting. However, conversion times and concentrations used in this article do not lead to a self-limiting effect. This is in contrast to the observations made by Campestrini et al. [52] on CCC on Alclad 2024-T3, where nucleation starts on IMPs and growth proceeds on the Al-matrix, enabling CCC to reach a greater thickness on the Al-matrix than on the IMPs after a longer conversion time. The probable reason for this is Zr's different hydrolysis and redox behaviour compared to Cr. The formation of CCC is controlled by pH and the concentration of reduced Cr(VI), and it exhibits more predictable hydrolysis behaviour. In contrast, the uncontrolled hydrolysis and condensation of Zr lead to overlapping nucleation and growth processes that occur on both the Al-matrix and IMPs with a longer conversion

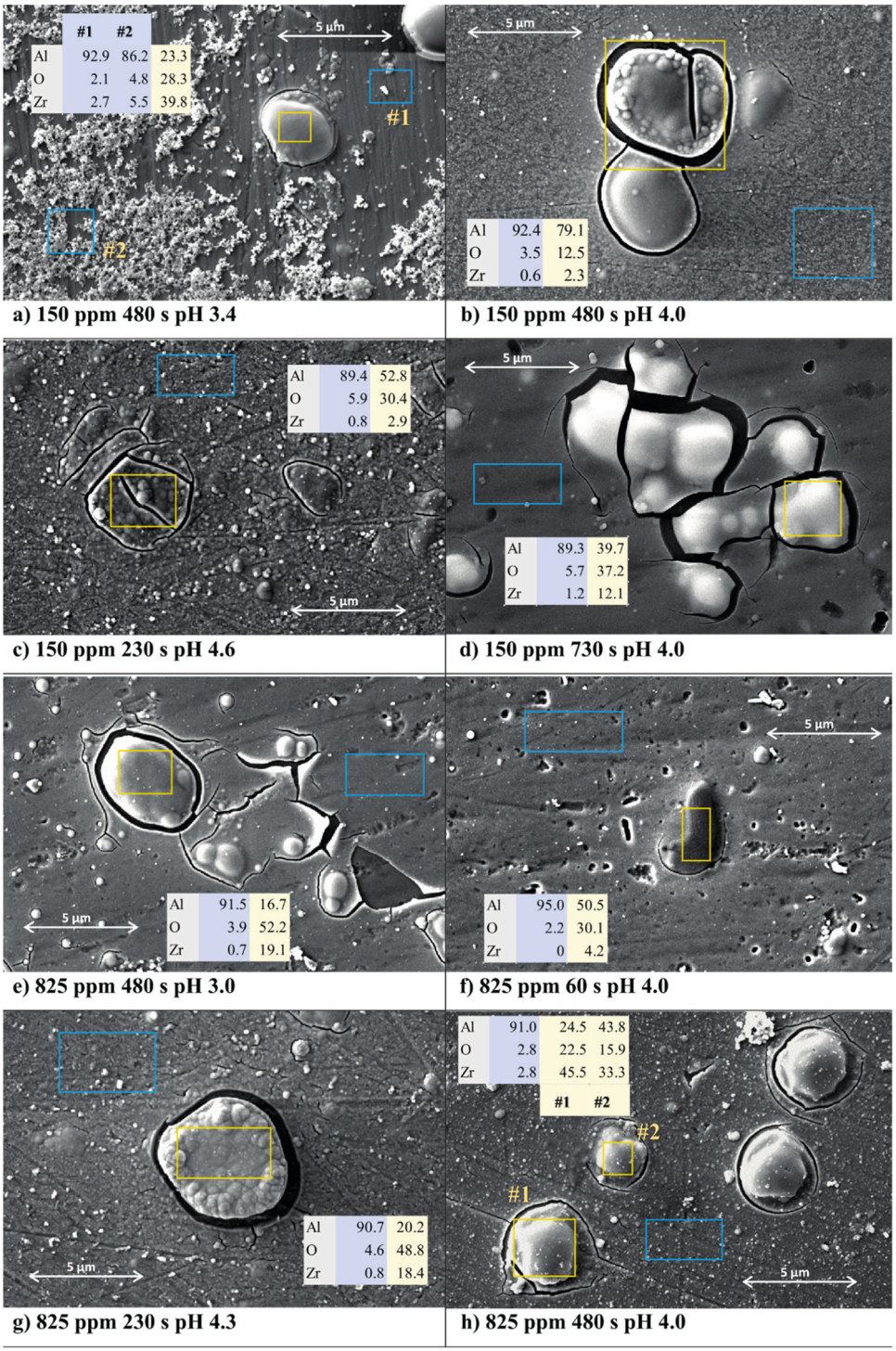


**Fig. 6.** SEM micrographs of AA5754 samples subjected to various ZrCC treatments. Blue and yellow rectangles note the locations of EDS analyses, and the results for Al, O, and Zr are given in tables (in at%). Blue sites belong to the matrix, and yellow sites correspond to intermetallic particles. All EDS results are given in the Supplementary material, Section 4.

time, with reduction currents not dependent on Zr concentration as much as on only pH.

However, the main influential factor for the conversion process on AA5754 is most certainly pH, as shown in the RSM plots (Figs. 3,4), as it governs the reactivity of Al-Fe IMPs. Performing the conversion process at low pH and higher concentration (825 ppm/480 s/pH 3.0 (Fig. 6e)) leads to lower Zr content on both the matrix and Al-Fe IMPs, as well as more pronounced cracking compared to all other samples at 825 ppm (Fig. 6h). On the other hand, a combination of low pH and concentration (150 ppm/480 s/pH 3.4 (Fig. 6a)) results in a high Zr content on both the Al-Fe IMP and the matrix, compared to other samples at 150 ppm (Fig. 6b-d). These samples exhibit a more uneven coating morphology with agglomerated zirconia nodules across the surface. This can be explained by starting the conversion process at a lower pH, which increases the cathodic reactivity of Fe-containing IMPs and the anodic activity of the subsequent aluminium matrix. A rapid accompanying formation of hydroxyls leads to localised alkalisation necessary for ZrCC deposition, albeit unevenly, leaving less time for uniform deposition of

zirconia and even leading to extensive agglomeration. Although 825 ppm/480 s/pH 3.0 (Fig. 6e) conditions on AA5754 did result in coating formation, unlike cold-rolled steel and Zn in our previous work [1], it can be concluded that, in general, the prevalence of anodic activity in the form of substrate dissolution during most of the conversion time outweighs the cathodic activity enabling ZrCC deposition. In other words, a longer time is required to achieve an equilibrium between substrate dissolution and ZrCC deposition at a pH $< 4$. Nevertheless, samples performed below pH 4 are not interesting from a corrosion standpoint and will not be further studied.

The first augmented sample, 825 ppm/230 s/pH 4.3 (Figs. S5 and 6), exhibits approximately half the amount of Zr compared to the central point, 825 ppm/480 s/pH 4.0, which can be attributed to a halved conversion time. Additionally, zirconia nodules are more concentrated at the edges of the IMPs, likely due to their proximity to the underlying cracks that facilitate cathodic reactions. Longer conversion times (480 s and beyond) lead to the creation of spherical particles by agglomerated $ZrO_2$ nodules (Fig. 6). pH of the 825 ppm/480 s/pH 4.3 sample is one coded unit (Supplementary material, Section 3) away from the best-performing pH of 4.6 and one coded unit away from the central point at pH 4.0. This suggests that the cathodic action of the IMPs does not undergo significant changes within this pH range. However, given the lower depletion rate of $H_2ZrF_6$ at higher concentrations and the fact that the ZrCC deposition always first starts at cathodic IMPs on aluminium alloys, with Zr deposition being greater at higher concentrations, it can be altogether inferred that the route for more accessible and better control of homogeneous ZrCC deposition on aluminium alloys is using low concentrations and pH values near zirconia precipitation.

Finally, the second augmentated sample (Fig. 3), carried out at a low concentration, shorter conversion time, and higher pH setting (150 ppm/230 s/pH 4.6), as guided by the first RSM augmentation (Fig. S6), yields the best performance in the drop test response (Table S3). This is further shown in SEM/EDS results (Fig. 6c), as the smallest difference in Zr content between the IMPs and matrix. Although some cracking is still present, which is likely a result of drying in SEM vacuum conditions or the fact that the coating is still too thick on the IMPs, the observed morphology corresponds to the best electrochemical behaviour (Fig. 1a). On the other hand, the obtained EIS data in the region of low concentration and higher pH imply that samples with medium conversion times (480 s) exhibit improved performance (Fig. 2). However, after observing the onset of cracking at IMPs already on the sample treated at 230 s, it can be noted that prolonged conversion times also lead to further cracking as ZrCC growth persists at IMPs. Thus, despite not achieving the best EIS performance (but near it) but the best drop test performance, the best-performing sample is, in our opinion, 150 ppm/230 s/ pH 4.6 (Fig. 6c). The need for augmentations, i.e., narrowing of the design space, confirms the anticipated higher sensitivity of AA5754 to changes in ZrCC bath parameters compared to CRS and Zn [1].

It should be noted that the present study confronted RSM principles, emphasising rapid and cost-effective result acquisition. Nonetheless, this approach carries the potential risk that the genuine effectiveness of ZrCCs might be compromised within a one-day timeframe. As demonstrated by Šekularac et al. [9–11], longer immersion times in a corrosive electrolyte generally yield increased impedance, sometimes surpassing ZrCC-free samples and reduced deviation in obtained impedances on a particular sample due to crack densification caused by corrosion products. This effect could be even more pronounced and favourable in the case of thicker coatings.

Therefore, in the context of AA5754, EIS measurements conducted within one day and near the best-performing region may exhibit heightened sensitivity for predicting future corrosion resistance compared to the drop test, as thicker coatings offer improved corrosion resistance under both short and extended immersion times. This highlights the need for further research on surface pretreatments before conversion. Additionally, to achieve better refinement in pH and conversion time at lower concentrations, implementing in-situ local electrochemical methods would be beneficial, which will be addressed in our future research. Nevertheless, in this case, RSM demonstrated particular benefits in determining the factor settings necessary for achieving the least-cracked coating, which had not been explicitly shown before.

### 3.4. Critical assessment of the results

The pH turns out to be the most critical factor for the conversion process on all substrates since it governs the cathodic control of corrosion reactions. Indeed, it has been shown earlier that the interfacial pH of electrochemical processes is significantly influenced by the underlying substrate [56]. We summarised the results obtained in this study with the comparative study on CRS and Zn from our previous study [1] in Table 3 to informatively present the responses and applicability of non-electrochemical and electrochemical methods on different substrates. In brief, the model for the PA after 10 min is suitable only for characterisation on CRS and AA5754, while the model for PA after 24 h can be used for both characterisation and optimisation. From PPC measurements, $R_p$ from Tafel extrapolation on Zn and AA5754 can be used for characterisation only. However, it seems like EIS arises as a mutual evaluation technique suitable for both characterisation and optimisation on all substrates, and care must be taken when choosing the type of resistance as a response, as it also differs between the substrates.

As the feasibility of certain responses varies with the substrate, it becomes clear that applying a one-size-fits-all optimisation strategy across different substrates is impractical as different techniques yield inconsistent results, heavily dependent on the substrate and any attempts at optimisation would need to be adjusted towards AA5754 at the expense of Zn and CRS. Overall, for CRS and Zn, where ZrCC deposition is guided by uniform corrosion [1], the best performance is achieved at moderate (825 ppm) to high concentrations (1226 ppm) and pH levels of 4.0–4.6. In contrast, for AA5754, where cathodic reaction kinetics are entirely influenced by IMPs achieving better control of deposition kinetics, lower concentrations (150 ppm), shorter to moderate conversion times (230–480 s), and elevated pH (4.0–4.6) are needed to acquire uniform coating deposition (Table 4). Additionally, medium immersion times at lower concentrations could have enhanced corrosion resistance at extended exposures to corrosive environments. While the coating formation on Zn and CRS is uniform, resulting from a continuous change of local anodic and cathodic sites, sustained spatial separation in AA5754 leads to substantial cracking after long conversion times, causing continuous cathodic action within the cracks.

It should be noted that the formation of nodular oxide structures, due to their porosity and catalytic activity, may promote further film growth through the enhancement of ORR [57] either on the oxide surface or substrate, as predicted by the porous oxide corrosion model [58]. Interestingly, it has been found that ZrCC nodules do not form on pure aluminium, which, along with the fact that in the case of aluminium alloys, nodular forms are present on IMPs more than matrix, points to

**Table 4**
Summary of governing mechanisms and best-performing factor ranges for ZrCCs deposition on different substrates (combining results from [1] and the current study).

| Mechanism | Substrate | Best-performing factor range | | |
|---|---|---|---|---|
| | | Conversion time | Concentration | pH |
| Governed by uniform corrosion | CRS | 480 s | 825 ppm–1226 ppm | 4.0–4.6 |
| | Zn | 480 s | 825 ppm–1226 ppm | 4.0–4.6 |
| Governed by cathodic action of IMPs | AA5754 | 230 s–480 s | 150 ppm | 4.0–4.6 |

electrocatalytic effects of ZrCC precipitation posed by IMPs, as shown by Chidambaram et al. [20]. Namely, if the growth rate of the film is significantly higher than the nucleation rate, nodular growth can be favoured when the deposition conditions or material itself lead to rapid film growth [59]. This is likely to be the case in ZrCC, given the aqueous behaviour of Zr [3].

The results imply that the Zr conversion process is primarily of a chemical rather than electrochemical nature, as demonstrated in previous studies on Cr-coatings by Zhang et al. [55] and further elaborated by Campestrini et al. [46,52]. Removing microgalvanic coupling between the IMPs and aluminium matrix would favour the sol-gel nature of the process and lead to more homogeneous coatings. This can be established, for example, by the control of density and electroactivity of IMPs [46,60] by application of electro-assisted deposition [61]. Nonetheless, all these findings emphasise the need for further investigations into the effect of conversion bath pH on different substrate materials. When the gelation phase of conversion coatings, like ZrCCs, is separate from drying (as in immersion application), initial products transform into stable forms through processes like Ostwald ripening. Prolonged exposure to air or baking dehydrates hydroxides into oxides, potentially impacting both ZrCC and the underlying substrate oxides. Unlike CCCs, which lose their self-healing ability at high temperatures due to the inability of Cr to migrate through the gel coating, Zr-based (as well as Ce-based) coatings require and can withstand higher drying temperatures [62,63]. However, the literature lacks a consensus on the specific drying conditions for ZrCCs, as the conditions appear arbitrary. Thus, further research is needed to establish standardized guidelines for ZrCC drying.

There seems to be a potential balance between the overall acidity of the solution, diminishing with higher pH and/or lower concentration and the time needed to achieve equilibrium between dissolution and precipitation. Importantly, achieving this equilibrium takes longer at lower pH values. This is further emphasised by the increased Zr availability near the surface at higher concentrations, leading to shorter yet effective conversion times, which improve corrosion protection.

Table 5 summarises the feasibility of individual techniques for the evaluation of different methods on different substrates. The drop test was more sensitive for CRS and Zn at a pH $<$ 4.0 and for AA5754 at a pH $\geq$ 4.0. Additionally, for Zn, the drop test conducted after air-drying for 24 h could only highlight the influence of pH. This suggests that a satisfactory coating forms at a higher pH (4.6), which is not necessarily related to its thickness. Combining PA trends from all substrates indicates that the drop test is predominantly influenced by the underlying substrate solubility, compactness, and Zr content rather than defects. Hence, samples treated at pH $<$ 4.0 on AA5754 also performed relatively well in the drop test because they have a high Zr content. However, the coating on these samples is the most non-uniform, as revealed by EIS and confirmed by SEM observations. In contrast, although EIS results are affected by charge transfer in large defects on AA5754, they also detect ZrCC thickness when the film is more uniform, especially at a lower concentration (150 ppm) and higher pH values (4.0; 4.6). This contrasts results for Zn and CRS in our previous article [1] and implies a greater long-term predictive capacity for EIS, recognising the influence of prolonged conversion time on thickness increase, resulting in improved corrosion resistance akin to AA5754. On the other hand, $R_p$ from Tafel extrapolation placed more emphasis on lower concentrations and shorter conversion times and was nevertheless deemed unsuitable by RSM models.

In the case of AA5754, however, $R_p$ from Tafel extrapolation produced RSM plots similar to EIS for AA5754 within a restricted experimental range of lower concentrations, conversion time, and higher pH. This suggests that $R_p$ might be a more suitable evaluation metric than $j_{corr}$ for PPC measurements, likely attributed to $R_p$ encompassing both thermodynamic and kinetic factors, enhancing its capacity to discern differences robustly. However, its feasibility for RSM models on all substrates was still poor, making it an unfeasible metric for evaluating ZrCC corrosion resistance (Table 5).

Further investigation using more sensitive techniques like local electrochemistry is needed to confirm model-suggested best-performing points and determine the best method for characterising ZrCCs on both substrates, which is planned for future research.

**Table 5**
Feasibility of individual techniques for evaluation of corrosion protection ability of ZrCCs on different substrates combining results from [1] and the current study.

| Technique | Benefits and drawbacks |
|---|---|
| **Drop test screening** | • More sensitive for CRS and Zn at pH $<$ 4<br>• More sensitive for AA5754 at pH $\geq$ 4 |
| **EIS** | • Dependent on the corrosion mechanism of the substrate<br>• High-frequency loop indicates sufficient ZrCC formation on CRS<br>• Highly dependent on the size of defects on AA5754<br>• Sensitive to ZrCC thickness on Zn at pH $\geq$ 4 and ZnO at pH $<$ 4 |
| **PPC** | • Not suitable for thin films<br>• Feasibility of PPC dependent on the nature of pores/cracks, i.e. if ZrCC is anodic or cathodic to the substrate |

## 4. Conclusions

This study extended the employment of RSM to comprehensively explore the experimental space, identify the best-performing conditions by adequately navigating the design space, and evaluate factor interactions, particularly on AA5754 substrate under diverse ZrCC bath conditions This approach also allowed for assessing the suitability of specific techniques and derived factors. The findings revealed that the drop test, after 24 h air-drying, can be an effective screening method for the ZrCC behaviour on AA5754 when combined with EIS due to its sensitivity and non-destructive nature. In contrast, when using PPC, polarisation resistance is a more convenient evaluation parameter compared to corrosion current density.

While PA assessment is inherently more subjective than electrochemical measurements, the drop test method is again advisable for a quick initial assessment of ZrCC performance. In particular, the drop test gives a generally accurate picture of ZrCC corrosion resistance at pH $\geq$ 4 on AA5754 substrate.

Regarding electrochemical measurements, EIS proved to be the most sensitive method for assessing interactions between conversion bath parameters across various combinations. From EIS results, it can be inferred that the ZrCC corrosion behaviour of AA5754 is exclusively controlled by charge transfer resistance. However, it does not always reflect the corrosion resistance behaviour of the AA5754-ZrCC in the whole experimental range, i.e., it requires narrowing it. In particular, on AA5754, EIS effectively characterises ZrCC only when complete coating formation is achieved (conversion time $\geq$ 230 s). Nevertheless, EIS displays the potential for effectively predicting prolonged corrosion performance depending on ZrCC thickness on AA5754 substrates at lower concentrations.

Moreover, in terms of the statistical applicability of the obtained RSM models, only those derived from EIS were shown to be able to function as a universal approach for both characterisation and, to a lesser extent, optimisation of all three substrates, CRS, Zn and AA5754, provided that the selection of the appropriate type of resistance from EIS as a response is carefully considered. Further investigation using more sensitive techniques like local electrochemistry is needed to confirm model-suggested best-performing points and determine the best method for characterising ZrCCs on all substrates.

This study also advocates the importance of selecting appropriate electrochemical measurements and electrolytes tailored to the specific system under investigation. Additionally, it highlights the necessity of assessing the corrosion performance of primers as a combination of ZrCC and underlying native oxide, especially in cases where the formed oxide does not crack. This knowledge can be extended further to formulate

individual baths with even more additives to obtain the desired performance and develop multi-metal coatings. Rather than delving deeply into the statistics of DoE and RSM, we intended to promote the more frequent application of DoE in corrosion research, enhancing the robustness of corrosion studies in general. RSM remains valuable for identifying best-performing regions and elucidating complex relationships between input factors and responses, ultimately contributing to assessing the extent of the viability of each evaluation technique.

Nevertheless, it must be remembered that interpreting results requires considering both statistical and practical significance in industrial applications. While larger sample sizes always increase the likelihood of detecting statistical significance, this does not necessarily translate to practical significance if the effect size is small. The latter often arises when values are of comparable magnitudes, leading to minor differences between observed samples that, despite being statistically significant, could lack practical importance. However, in this case, assessing statistical significance proved valuable in unveiling process behaviour, at least from a fundamental level. In other words, to echo the sentiments of George Box, a pioneer in experimental design: "All models are wrong, but some are useful [64]."

## Funding

This research was funded by the Slovenian Research and Innovation Agency (research core funding grants P2–0393 and P2–0266 and project PR-09806).

## Author statement

All persons who meet authorship criteria are listed as authors, and all authors certify that they have participated sufficiently in the work to take public responsibility for the content, including participation in the concept, design, analysis, writing, or revision of the manuscript.

The authors declare that the science contained in this manuscript has not been previously published and is not under consideration by any other journal.

## CRediT authorship contribution statement

**Kras Ana:** Writing – review & editing, Writing – original draft, Methodology, Investigation, Formal analysis, Conceptualization. **Kramar Davorin:** Writing – review & editing, Writing – original draft, Validation, Methodology, Conceptualization. **Milosev Ingrid:** Writing – review & editing, Writing – original draft, Validation, Supervision, Project administration, Methodology, Conceptualization.

## Declaration of Competing Interest

The author declare that they have no known competing financial interests or personal relationships that could have appeared to influence the work reported in this paper.

## Acknowledgements

Financial support for this study was provided by the Slovenian Research and Innovation Agency (see Funding section). The authors extend their sincere appreciation to Dr. Neil Spinner of Pine Research Instrumentation, Inc., for conducting insightful webinars that not only were cost-free but also imparted valuable knowledge. These webinars were instrumental in laying a solid foundation for a more thorough exploration of EIS literature and for accurately interpreting EIS spectra. Special thanks go to Dimitrij Us, MSc, and Dr. Sabina Ovčjak from SurTec Adria d.o.o. for their generous guidance in preparing ZrCCs and sharing their invaluable industry expertise. The authors also recognise Dr. Iosif Fromondi from Methrom Autolab for his consistent availability and generous support in utilising Autolab and NOVA, particularly for his guidance in EIS fitting within NOVA, which proved invaluable. A. Kraš expresses sincere gratitude to Prof. Davor Dolar and Dr. Marko Racar for their invaluable introduction to Response Surface Methodology (RSM) during undergraduate studies at the University of Zagreb, Faculty of Chemical Engineering and Technology. Lastly, heartfelt gratitude is expressed to Barbara Kapun, BSc., for her prompt SEM/EDS analyses and engaging discussions.

## Appendix A. Supporting information

Supplementary data associated with this article can be found in the online version at doi:10.1016/j.corsci.2025.112824.

## Data availability

Data will be made available on request.

## References

[1] A. Kraš, D. Kramar, I. Milošev, Characterisation of the deposition and protection performance of Zr conversion coatings on steel and zinc substrates using the response surface methodology, Corros. Sci. 242 (2024) 112551, https://doi.org/10.1016/j.corsci.2024.112551.
[2] W.S. Miller, L. Zhuang, J. Bottema, A.J. Wittebrood, P. De Smet, A. Haszler, A. Vieregge, Recent development in aluminium alloys for the automotive industry, Mater. Sci. Eng. A 280 (2000) 37–49, https://doi.org/10.1016/S0921-5093(99)00653-X.
[3] A. Kraš, I. Milošev, The aqueous chemistry of zirconium as a basis for better understanding the formation of zirconium conversion coatings: Updated thermodynamic data, J. Electrochem. Soc. 170 (2023) 21508, https://doi.org/10.1149/1945-7111/acb9c2.
[4] A. Kraš, I. Milošev, Comparative electrochemical and thermodynamic study of cold-rolled steel, Al alloy AA5754, and Zn corrosion in fluoride and chloride solutions, Electrochim. Acta 502 (2024) 144819, https://doi.org/10.1016/j.electacta.2024.144819.
[5] M.J. Anderson, P.J. Whitcomb. DOE Simplified, 3rd ed., Productivity Press, New York, 2017 https://doi.org/10.1201/b18479.
[6] M.J. Anderson, P.J. Whitcomb. RSM Simplified, 2nd ed., Productivity Press, New York, 2016 https://doi.org/10.1201/9781315382326.
[7] D. Kramar, Process modelling using design of experiments, in: G. Globočki-Lakić, D. Kramar, J. Kopač (Eds.), Metal Cutting-Theory and Applications, Faculty of Mechanical Engineering, University of Banja Luka and Faculty of Mechanical Engineering, University of Ljubljana, Banja Luka and Ljubljana, 2014.
[8] I. Milošev, G.S. Frankel, Review—conversion coatings based on zirconium and/or titanium, J. Electrochem. Soc. 165 (2018) C127–C144, https://doi.org/10.1149/2.0371803jes.
[9] G. Šekularac, J. Kovač, I. Milošev, Comparison of the electrochemical behaviour and self-sealing of zirconium conversion coatings applied on aluminium alloys of series 1xxx to 7xxx, J. Electrochem. Soc. 167 (2020) 111506, https://doi.org/10.1149/1945-7111/aba875.
[10] G. Šekularac, I. Milošev, Electrochemical behavior and self-sealing ability of zirconium conversion coating applied on aluminum alloy 3005 in 0.5 M NaCl solution, J. Electrochem. Soc. 167 (2020) 021509, https://doi.org/10.1149/1945-7111/ab6b0d.
[11] G. Šekularac, J. Kovač, I. Milošev, Prolonged protection, by zirconium conversion coatings, of AlSi7Mg0.3 aluminium alloy in chloride solution, Corros. Sci. 169 (2020) 108615, https://doi.org/10.1016/j.corsci.2020.108615.
[12] M. Mujdrica Kim, B. Kapun, U. Tiringer, G. Šekularac, I. Milošev, Protection of aluminum alloy 3003 in sodium chloride and simulated acid rain solutions by commercial conversion coatings containing Zr and Cr, Coatings 9 (2019) 563, https://doi.org/10.3390/coatings9090563.
[13] F.L. Floyd, S. Avudaiappan, J. Gibson, B. Mehta, P. Smith, T. Provder, J. Escarsega, Using electrochemical impedance spectroscopy to predict the corrosion resistance of unexposed coated metal panels, Prog. Org. Coat. 66 (2009) 8–34, https://doi.org/10.1016/j.porgcoat.2009.04.009.
[14] F.L. Floyd, S. Tatti, T. Provder, Using DC electrochemical techniques to assess the relative corrosiveness of water-based coatings and their ingredients, J. Coat. Technol. Res. 4 (2007) 111–129, https://doi.org/10.1007/s11998-007-9012-5.
[15] ГОСТ 9.302-88, Edinaya sistema zashchity ot korrozii i stareniya. Pokrytiya metallicheskie i nemetallicheskie neorganicheskie, Metody kontrolya, Izd, Standardov, Moscow, 1990.
[16] F.D. Timmins, Avoiding Paint Failures by Prohesion, J. Oil Col. Chem. Assoc. 62 (1979) 131–135.
[17] K. Ogle, R.G. Buchheit, Conversion coatings, in: A.J. Bard, M. Stratmann (Eds.), Encyclopedia of Electrochemistry, Wiley-VCH, Weinheim, 2003, https://doi.org/10.1002/9783527610426.bard040503.
[18] Regulation (EC) No 1907/2006 of the European Parliament and of the Council of 18 December 2006 concerning the Registration, Evaluation, Authorisation and Restriction of Chemicals (REACH), 2014 (2023).

[19] S. Mancini, Conversion coatings: Phosphate vs. zirconium, Products Finishing, 2018. ⟨https://www.pfonline.com/articles/conversion-coatings-phosphate-vs-zirconium⟩- (accessed October 18, 2023).

[20] D. Chidambaram, C.R. Clayton, G.P. Halada, The role of hexafluorozirconate in the formation of chromate conversion coatings on aluminum alloys, Electrochim. Acta 51 (2006) 2862–2871, https://doi.org/10.1016/j.electacta.2005.08.022.

[21] K. Ogle, M. Wolpers, Phosphate conversion coatings, in: S.D. Cramer, B.S. Covino (Eds.), Corrosion: Fundamentals, Testing, and Protection, ASM International, 2003, pp. 712–719, https://doi.org/10.31399/asm.hb.v13a.a0003678.

[22] ASTM International, ASTM F22-21, Standard test method for hydrophobic surface films by the water-break test, 2021. https://doi.org/10.1520/F0022-21.

[23] G.S. Frankel, M. Rohwerder, Electrochemical techniques for corrosion, in: M. Stratmann, G.S. Frankel (Eds.), Encyclopedia of Electrochemistry, Wiley, Weinheim, 2003, https://doi.org/10.1002/9783527610426.bard040007.

[24] R.G. Kelly, J.R. Scully, D. Shoesmith, R.G. Buchheit, Electrochemical Techniques in Corrosion Science and Engineering, CRC Press, Boca Raton, FL, 2002, https://doi.org/10.1201/9780203909133.

[25] ASTM International, ASTM G59-97(2020), Standard test method for conducting potentiodynamic polarization resistance measurements, 2023. https://doi.org/10.1520/G0059-97R20.

[26] M.E. Orazem, B. Tribollet, Electrochemical Impedance Spectroscopy, Wiley, Hoboken, New Jersey, 2008, https://doi.org/10.1002/9780470381588.

[27] D.H. van der Weijde, E.P.M. van Westing, J.H.W. de Wit, Electrochemical techniques for delamination studies, Corros. Sci. 36 (1994) 643–652, https://doi.org/10.1016/0010-938X(94)90070-1.

[28] E. Barsoukov, J.R. Macdonald, Impedance Spectroscopy, Wiley, Hoboken, New Jersey, 2005, https://doi.org/10.1002/0471716243.

[29] D.D. Macdonald, M. Urquidi-Macdonald, Theory of steady-state passive films, J. Electrochem. Soc. 137 (1990) 2395–2402, https://doi.org/10.1149/1.2086949.

[30] R.G. Buchheit, M. Cunningham, H. Jensen, M.W. Kendig, M.A. Martinez, A correlation between salt spray and electrochemical impedance spectroscopy test results for conversion-coated aluminum alloys, Corrosion 54 (1998) 61–72, https://doi.org/10.5006/1.3284829.

[31] J.M. Hu, J.Q. Zhang, C.N. Cao, Determination of water uptake and diffusion of $Cl^-$ ion in epoxy primer on aluminum alloys in NaCl solution by electrochemical impedance spectroscopy, Prog. Org. Coat. 46 (2003) 273–279, https://doi.org/10.1016/S0300-9440(03)00010-9.

[32] D. Peng, J. Wu, X. Yan, X. Du, Y. Yan, X. Li, The formation and corrosion behavior of a zirconium-based conversion coating on the aluminum alloy AA6061, J. Coat. Technol. Res. 13 (2016) 837–850, https://doi.org/10.1007/s11998-016-9789-1.

[33] G.E.P. Box, W.G. Hunter, S.J. Hunter, Statistics for Experimenters: Design, Innovation, and Discovery, Wiley, New York, 2005.

[34] J. Konopka, Examination of the fluorine K line and iron L line overlap by EDS and WDS, Application Note 52455, Madison, WI, USA, 2013. ⟨www.thermoscientific.com⟩.

[35] J.I. Goldstein, D.E. Newbury, J.R. Michael, N.W.M. Ritchie, J.H.J. Scott, D.C. Joy, Scanning Electron Microscopy and X-Ray Microanalysis, Springer New York, New York, NY, 2018, https://doi.org/10.1007/978-1-4939-6676-9.

[36] R.K. Mishra, A.K. Zachariah, S. Thomas, Energy-dispersive X-ray spectroscopy techniques for nanomaterials. Microscopy Methods in Nanomaterials Characterization, Elsevier, 2017, pp. 383–405, https://doi.org/10.1016/B978-0-323-46141-2.00012-2.

[37] A. Afseth, J.H. Nordlien, G.M. Scamans, K. Nisancioglu, Effect of heat treatment on electrochemical behaviour of aluminium alloy AA3005, Corros. Sci. 44 (2002) 145–162, https://doi.org/10.1016/S0010-938X(01)00024-5.

[38] O. Engler, K. Kuhnke, J. Hasenclever, Development of intermetallic particles during solidification and homogenization of two AA 5xxx series Al-Mg alloys with different Mg contents, J. Alloy. Compd. 728 (2017) 669–681, https://doi.org/10.1016/j.jallcom.2017.09.060.

[39] Z. Jin, C. Cai, Y. Yuan, D. Kang, J. Hunter, X. Zhou, The behaviour of AA5754 and AA5052 aluminium alloys in alkaline etching solution: Similarity and difference, Mater. Charact. 171 (2021) 110768, https://doi.org/10.1016/j.matchar.2020.110768.

[40] Z. Jin, C. Cai, T. Hashimoto, Y. Yuan, D. Kang, J. Hunter, X. Zhou, The behaviour of iron-containing intermetallic particles in aluminium alloys in alkaline solution, Corros. Sci. 179 (2021) 109134, https://doi.org/10.1016/j.corsci.2020.109134.

[41] N. Birbilis, R.G. Buchheit, Investigation and discussion of characteristics for intermetallic phases common to aluminum alloys as a function of solution pH, J. Electrochem. Soc. 155 (2008) C117, https://doi.org/10.1149/1.2829897.

[42] T. Kosec, D.K. Merl, I. Milošev, Impedance and XPS study of benzotriazole films formed on copper, copper–zinc alloys and zinc in chloride solution, Corros. Sci. 50 (2008) 1987–1997, https://doi.org/10.1016/j.corsci.2008.04.016.

[43] P. Campestrini, E.P.M. van Westing, H.W. van Rooijen, J.H.W. de Wit, Relation between microstructural aspects of AA2024 and its corrosion behaviour investigated using AFM scanning potential technique, Corros. Sci. 42 (2000) 1853–1861, https://doi.org/10.1016/S0010-938X(00)00002-0.

[44] L.F. Mondolfo, Aluminum Alloys, Elsevier, London, UK, 1976, https://doi.org/10.1016/C2013-0-04239-9.

[45] I. Milošev, B. Kapun, P. Rodič, The relation between the microstructure of aluminum alloy 7075-T6 and the type of cerium salt in the formation of the cerium conversion layer, J. Electrochem. Soc. 169 (2022) 091501, https://doi.org/10.1149/1945-7111/ac8d35.

[46] P. Campestrini, E.P.M. van Westing, J.H.W. de Wit, Influence of surface preparation on performance of chromate conversion coatings on Alclad 2024 aluminium alloy: Part I: Nucleation and growth, Electrochim. Acta 46 (2001) 2553–2571, https://doi.org/10.1016/S0013-4686(01)00475-3.

[47] K.F. Lorking, J.E.O. Mayne, The corrosion of aluminium in solutions of sodium fluoride and sodium chloride, Br. Corros. J. 1 (1966) 181–182, https://doi.org/10.1179/000705966798327795.

[48] A.F. Beck, M.A. Heine, D.S. Keir, D. van Rooyen, M.J. Pryor, Further studies of the electrical characteristics of oxide films on aluminium, Corros. Sci. 2 (1962) 133–145, https://doi.org/10.1016/0010-938X(62)90005-7.

[49] T. Xue, W.C. Cooper, R. Pascual, S. Saimoto, Effect of fluoride ions on the corrosion of aluminium in sulphuric acid and zinc electrolyte, J. Appl. Electrochem. 21 (1991) 238–246, https://doi.org/10.1007/BF01052577.

[50] H. Eivaz Mohammadloo, A.A. Sarabi, R. Mohammad Hosseini, M. Sarayloo, H. Sameie, R. Salimi, A comprehensive study of the green hexafluorozirconic acid-based conversion coating, Prog. Org. Coat. 77 (2014) 322–330, https://doi.org/10.1016/j.porgcoat.2013.10.006.

[51] A. Niaz, Complementary use of electrochemical testing techniques to study corrosion processes of HVOF Inconel 625, CoNiCrAlY and WCCoCr coatings, PhD Thesis, University of Nottingham, 2013.

[52] P. Campestrini, H. Terryn, J. Vereecken, J.H.W. de Wit, Chromate conversion coating on aluminum alloys: II: Effect of the microstructure, J. Electrochem. Soc. 151 (2004) B359, https://doi.org/10.1149/1.1736682.

[53] C.J. Brinker, G.W. Scherer. Sol-Gel Science: The Physics and Chemistry of Sol-Gel Processing, 1st ed., Academic Press, Boston, 1990.

[54] P. Campestrini, G. Goeminne, H. Terryn, J. Vereecken, J.H.W. de Wit, Chromate conversion coating on aluminum alloys: I. Formation mechanism, J. Electrochem. Soc. 151 (2004) B59, https://doi.org/10.1149/1.1637355.

[55] W. Zhang, B. Hurley, R.G. Buchheit, Characterization of chromate conversion coating formation and breakdown using electrode arrays, J. Electrochem. Soc. 149 (2002) B357, https://doi.org/10.1149/1.1485774.

[56] S. Díaz, ZnFe anomalous electrodeposition: stationaries and local pH measurements, Electrochim. Acta 47 (2002) 4091–4100, https://doi.org/10.1016/S0013-4686(02)00416-4.

[57] S. Thomas, I.S. Cole, M. Sridhar, N. Birbilis, Revisiting zinc passivation in alkaline solutions, Electrochim. Acta 97 (2013) 192–201, https://doi.org/10.1016/j.electacta.2013.03.008.

[58] M.S. Venkatraman, I.S. Cole, B. Emmanuel, Corrosion under a porous layer: a porous electrode model and its implications for self-repair, Electrochim. Acta 56 (2011) 8192–8203, https://doi.org/10.1016/j.electacta.2011.06.020.

[59] G. Cao, Y. Wang, Nanostructures and Nanomaterials, World Scientific, Singapore, 2011, https://doi.org/10.1142/7885.

[60] P. Campestrini, E.P.M. van Westing, J.H.W. de Wit, Influence of surface preparation on performance of chromate conversion coatings on Alclad 2024 aluminium alloy: Part II: EIS investigation, Electrochim. Acta 46 (2001) 2631–2647, https://doi.org/10.1016/S0013-4686(01)00476-5.

[61] V. Bonamigo Moreira, A. Puiggalí-Jou, E. Jiménez-Piqué, C. Alemán, A. Meneguzzi, E. Armelin, Green nanocoatings based on the deposition of zirconium oxide: the role of the substrate, Materials 14 (2021) 1043, https://doi.org/10.3390/ma14041043.

[62] T.G. Harvey, Cerium-based conversion coatings on aluminium alloys: a process review, Corros. Eng. Sci. Technol. 48 (2013) 248–269, https://doi.org/10.1179/1743278213Y.0000000089.

[63] J.H. Osborne, Observations on chromate conversion coatings from a sol–gel perspective, Prog. Org. Coat. 41 (2001) 280–286, https://doi.org/10.1016/S0300-9440(01)00143-6.

[64] G.E.P. Box, Science and statistics, J. Am. Stat. Assoc. 71 (1976) 791–799, https://doi.org/10.1080/01621459.1976.10480949.